ACS OMEGA

Article

http://pubs.acs.org/journal/acsodf

Surfactant-Mediated One-Pot Method To Prepare Pd−CeO_2 Colloidal Assembled Spheres and Their Enhanced Catalytic Performance for CO Oxidation

Chenhao Du, Guanzhong Lu,* Yun Guo, Yanglong Guo, and Xue-qing Gong

Key Laboratory for Advanced Materials and Research Institute of Industrial Catalysis, School of Chemistry and Molecular Engineering, East China University of Science and Technology, 130 Meilong Road, Shanghai 200237, P. R. China

S *Supporting Information*

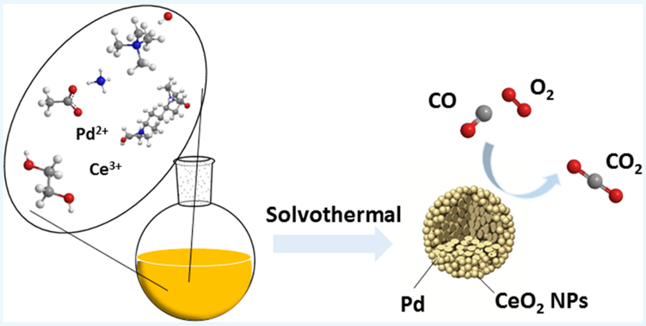

ABSTRACT: A simple, one-pot method to fabricate ordered, monodispersed Pd−CeO_2 colloidal assembled spheres (CASs) was developed using the surfactant-mediated solvothermal approach, which involves a tunable self-assembled process by carefully controlling different chemical reactions. The evolution process and formation mechanism of the CASs were thoroughly investigated by time-controlled and component-controlled experiments. For CO oxidation, this CAS nanocatalyst exhibited much higher catalytic activity and thermal stability than Pd/CeO_2 prepared by an impregnation method, and its complete CO conversion temperature is ~120 °C. The enhanced catalytic performance for CO oxidation could be attributed to the synergistic effect of highly dispersed PdO species and Pd^{2+} ions incorporated into the CeO_2 lattice. For this CAS catalyst, each sphere can be viewed as a single reactor, and its catalytic performance can be further improved after being supported on alumina, which is obviously higher than results previously reported. Furthermore, this method was used to successfully prepare M−CeO_2 CASs (M = Pt, Cu, Mn, Co), showing further that this is a new and ideal approach for fabricating active and stable ceria-based materials.

1. INTRODUCTION

Pd-based catalysts have been intensively researched in recent years because of their wide applications in various catalytic processes.[1−4] For example, Pd-catalyzed carbon−carbon cross-coupling reactions are the most important and practical reactions in organic chemistry.[5,6] Supported PdO_x species have been recognized as the active sites for CH_4 combustion, and an application of Pd-only three-way catalysts represents a meaningful progress for the removal of pollutants from exhaust gas.[7,8] It is known that the catalytic activity of Pd nanoparticles (NPs) is closely related to their size, shape, and valence state;[9−12] thus it is of great importance to maintain the morphology or physicochemical states of Pd-active species under various reaction conditions. For this purpose, Pd NPs are often loaded on supports, such as metal oxides, zeolites, carbon materials, and so forth. Among these kinds of supports, cerium oxide is considered as a unique one because of its oxygen storage/release capacity and its redox capability to influence the chemical and electronic states of Pd species.[13]

Pd/CeO_2 has been widely researched and used in various catalytic reactions, such as three-way catalytic exhaust gas purification, volatile organic compound (VOC) elimination, selective hydrogenations, and photocatalytic reactions.[14−19] In recent years, with the help of advanced nanomaterial synthesis technology, it is now possible to purposefully design Pd−CeO_2 hybrid nanocatalysts with unique features and further improve their functionality.[20−24] For instance, Cargnello et al. designed and prepared a Pd@CeO_2-type catalyst by means of the concepts of supramolecular chemistry and showed an exceptional activity and stability in methane combustion.[25−27] Zhang et al. explored a clean synthesis of high-quality Pd@CeO_2 nanospheres by salting-out-assisted growth and self-assembly, which improved their catalytic activity for CO oxidation.[28] They recently also fabricated a Pd@CeO_2 hybrid structure with tunable Pd core sizes with a simple two-step biomolecular-assisted process without any expensive or toxic ligand.[29] We have synthesized a hollow-structured core−shell-like Pd−CeO_2 nanocomposite by the hard-template method, which exhibited enhanced catalytic activities for CO oxidation and selective reduction of 4-nitrophenol. The Pd particles can be well protected by the CeO_2 shell, and the catalytic stability could be well maintained even after calcination at 700 °C.[30]

Although many gratifying achievements have been made, there are still some challenges remaining. In Cargnello's protocol, multiple procedures are needed to obtain the hybrid structures, which is time consuming, inevitably. Besides, large amounts of toxic organic solvents and surfactants are required during the assembly processes. In Zhang's process, the size of Pd NPs is

Received: May 14, 2016
Accepted: June 27, 2016
Published: July 19, 2016

DOI: 10.1021/acsomega.6b00050
ACS Omega 2016, 1, 118−126

relatively large (>8 nm); thus, the utilization of the Pd element is not efficient enough. Therefore, it is still necessary to develop simple and green methods for preparing highly active Pd−CeO_2 hybrid nanocatalysts with more efficient Pd utilization.

With the help of the hands-on experience of researchers, the key factors for successfully synthesizing novel Pd−CeO_2 hybrid structures include the manipulation of individual chemical reactions rates, especially tuning interfacial chemical processes among different components. In this paper, we developed a one-pot, surfactant-assisted solvothermal method to prepare Pd−CeO_2 colloidal assembled spheres (CASs). The Pd clusters were dispersively distributed in CeO_2 CASs by a one-pot method, which is more efficient than some of the two-step processes to prepare noble-metal/oxide nanospheres.[31,32] The results showed that the Pd−CeO_2 CAS superstructure exhibited an enhanced catalytic activity for CO oxidation compared with a conventional Pd/CeO_2-supported catalyst. Moreover, this method can be easily extended to the synthesis of Pt−CeO_2 CASs and transition metal-incorporated CeO_2 CASs.

2. EXPERIMENTAL SECTION

2.1. Sample Synthesis. *Pd−CeO_2 CASs.* $CeCl_3·7H_2O$ was dissolved in ethylene glycol (6 g $CeCl_3·7H_2O$ per 100 mL of solvent) under stirring for 2 h. $CeCl_3·7H_2O$ ethylene glycol solution (10 mL) and 30 mL ethylene glycol were added into a 250 mL flask under stirring at room temperature. Then a certain amount of K_2PdCl_4 was added under intensive stirring for 30 min, followed by adding 0.1 g of polyvinylpyrrolidone (PVP), 2 mL of acetic acid, 0.5 mL of tetramethylammounium hydroxide ($N(CH_3)_4OH$, 25% in H_2O), and 0.4 mL of concentrated ammonia hydroxide (25−28% in H_2O), forming a transparent light-brown solution. This solution was immersed in an oil bath, and the temperature was increased up to 130 °C; a grayish suspension solution was obtained after 15 h of the reaction.

After the reaction was completed and cooled down to room temperature, this mixture was diluted with 40 mL of acetone and then centrifuged at 4500 rpm for 15 min. The resulted solid was dispersed in the mixed solution of acetone and ethanol (v/v = 1:1), followed by centrifugation twice at 4000 rpm for 10 min. The obtained product was dried at 60 °C overnight and calcined at 600 °C for 2 h.

Pd−CeO_2 CAS Supported on γ-Al_2O_3. A certain amount of γ-Al_2O_3 was dispersed in 50 mL of deionized water under ultrasonication for 10 min. A calcined Pd−CeO_2 CAS suspension (20 mL, 2.5 mg/mL) was slowly added into the Al_2O_3 solution under stirring at room temperature for 1 h. The product was gathered by centrifugation and dried at 80 °C overnight.

Pd/CeO_2-Imp Catalyst. The conventional Pd/CeO_2 catalyst was prepared by the impregnation method with $PdCl_2$ as the precursor. The collected powder was dried at 80 °C and calcined at 600 °C for 2 h.

Pt−CeO_2 CASs. K_2PtCl_4 was used as a precursor instead of K_2PdCl_4. The preparation reaction was conducted at 140 °C for 20 h, and other processes were the same as those of Pd−CeO_2 CASs.

Transition Metal (M = Cu, Co, Mn)−CeO_2 CASs (M−CeO_2 CASs). $CuCl_2$, $CoCl_2$, and $Mn(CH_3COO)_2$ were used as precursors with a molar ratio of 1:9 (transition metal: Ce), and the synthesis processes were the same as those of Pd−CeO_2 CASs except the addition of PVP. For the Mn−CeO_2 CAS sample, the reaction time was prolonged to 24 h.

2.2. Catalytic Activity Testing. The catalytic performances of samples for CO oxidation were evaluated in a fixed-bed reactor. For a typical testing, the Pd−CeO_2 catalyst diluted with silica was loaded in a quartz-tube reactor. Then, the feed gas containing 1 vol % CO, 20 vol % O_2, and balance N_2 was introduced into the reactor at a flow rate of 50 mL/min. After the sample was pretreated in 10 vol % O_2/N_2 at 150 °C for 30 min, the temperature of the reactor was raised at a rate of 2 °C/min from room temperature. The gas composition was monitored online using a GC (GC 2060 system) with a flame ionization detector (FID) and methane converter. The conversion of CO was calculated on the basis of the change of CO concentrations in the inlet and outlet gases.

Kinetic experiments were performed at a gas hourly space velocity (GHSV) of 100 000 or 150 000 mL/(g_{cat}·h). Typical conversions of CO were kept well below 10% so that the differential conditions could be assumed.

The stability testing was performed under a cycling experiment. Before the testing, the catalyst was pretreated in the feed gas at 600 °C for 30 min and then cooled down to 85 °C to test the conversion of CO to CO_2. The cycle was repeated three times.

Turnover frequency (TOF) measurements were conducted at 60 °C at a GHSV of 100 000 mL/(g_{cat}·h). The CO conversion was obtained after 20 min of the CO reaction, and the TOF was calculated based on the equation $\mathrm{TOF} = \frac{X_{CO}V_{CO}N_A}{N}$, where X_{CO} is the CO conversion, V_{CO} is the gas flow of CO (mol/s), N_A is the Avogadro constant, and N is the number of the catalytic sites ($N = N_t·D_{Pd}$, where N_t is the total amount of Pd atom in the catalyst and D_{Pd} is the Pd dispersion).

2.3. Characterization of Samples. Elemental analysis of the sample was done by inductively coupled-plasma atomic emission spectroscopy (ICP-AES) on a Varian 710ES instrument (Varian Co. Palo Alto, US). Powder X-ray diffraction (XRD) patterns were recorded on a PANalytical PW 3040/60 X'Pert Pro powder diffractometer with Cu Kα radiation, which was operated at 40 kV and 40 mA and a scanning speed of 0.5°/min. N_2 adsorption/desorption isotherms of samples were measured at −196 °C on a micromeritics ASAP 2020 instrument, and the surface area was calculated by the Brunauer−Emmett−Teller (BET) method. The Pd dispersion in the catalysts was calculated by the CO chemisorption method on AutoChem II 2920 chemical adsorption equipment at room temperature.

H_2 temperature-programmed reduction (H_2-TPR) was carried on a PX200 apparatus (Tianjin Pengxiang Technology Co. Ltd.) with a thermal conductivity detector (TCD). The catalyst (40 mg) was used, and the reduction gas consisted of 5% H_2/N_2 with a flow rate of 40 mL/min. TPR was run from room temperature to 800 °C at 10 °C/min.

Transmission electron microscopy (TEM) images were taken on a JEM-2100 transmission electron microscope. The sample was ultrasonically suspended in the ethanol solvent, and one or two drops of this slurry were deposited on a copper grid. The liquid phase was evaporated before the grid was loaded into the microscope.

The X-ray photoelectron spectroscopy (XPS) spectra of samples were obtained on a Kratos Axis Ultra-DLD photoelectron spectrometer equipped with Al Kα (1486.6 eV) radiation as the excitation source. All binding energies (BEs) were determined with respect to the C1s line (284.8 eV) originating from adventitious carbon.

The size distribution of spheres was measured by photon correlation spectroscopy on a Zetasizer instrument (Malvern Instruments Ltd.) at room temperature. The suspension was

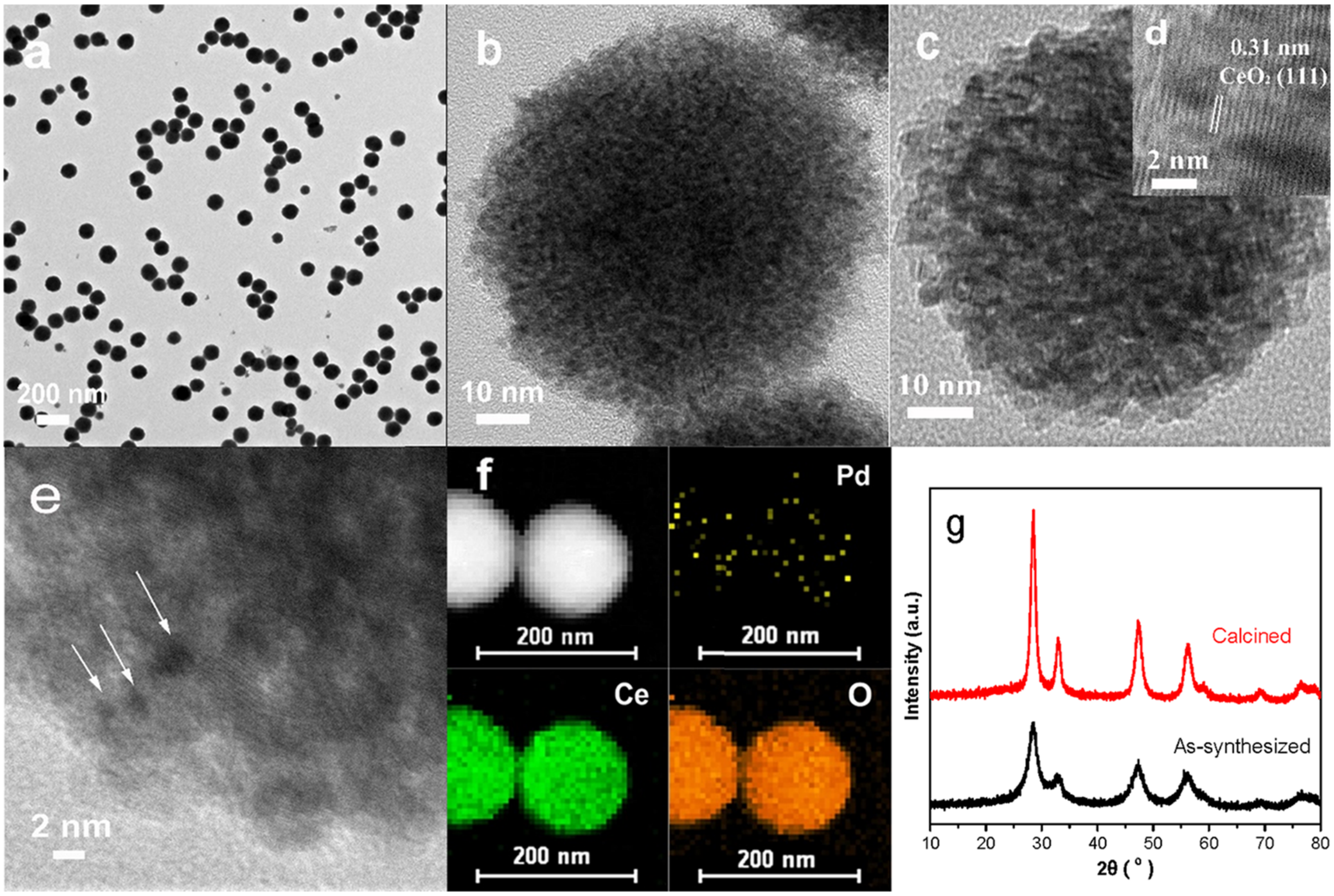

Figure 1. TEM images of (a,b) the as-prepared Pd−CeO_2 CASs, (c−e) sample calcined at 600 °C, (f) STEM image and elemental mapping of Pd−CeO_2 CASs, and (g) XRD profiles of the as-prepared and calcined Pd−CeO_2 CASs.

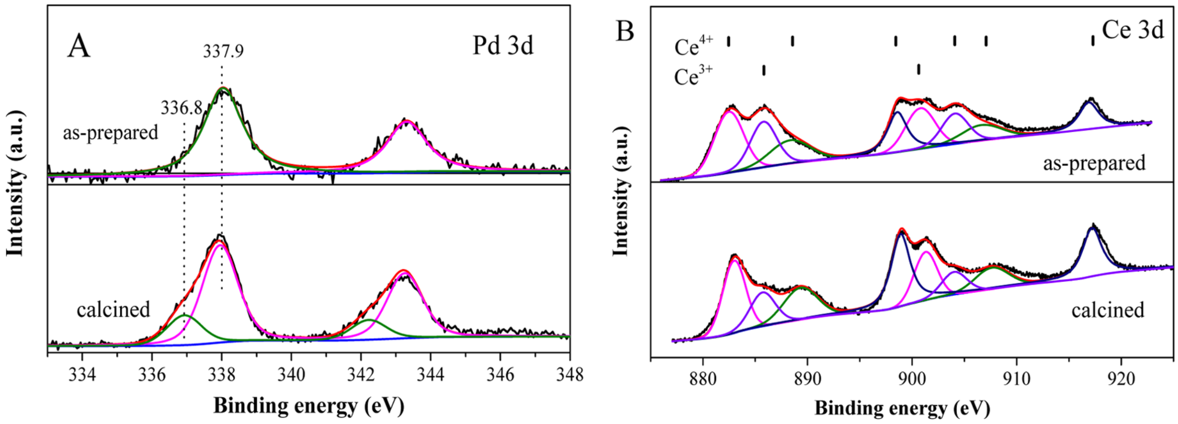

Figure 2. (A) Pd 3d and (B) Ce 3d XPS spectra of the as-synthesized and calcined Pd−CeO_2 CASs at 600 °C.

prepared with a concentration of 0.5 mg/mL followed by ultrasonication for 15 min.

3. RESULTS AND DISCUSSION

The Pd−CeO_2 CASs were synthesized in a simple one-pot fashion by the modified solvothermal method. As shown in TEM images (Figure 1a,b) and size distribution profiles (Figure S1), the as-synthesized Pd−CeO_2 CASs are well monodispersed, and their average size is 100−120 nm. The as-synthesized hybrid spheres are composed mainly of small 2−3 nm CeO_2 nanocrystals, which is consistent with the XRD results (Figure 1g). However, the dense stacking of CeO_2 nanocrystals makes it difficult to discern the distribution of Pd species in the spheres, so high-angle annular dark-field scanning transmission electron microscopy (HAADF-STEM) was used to illustrate the mappings of Pd, Ce, and O components in the CAS. As shown in Figure 1f, Pd is randomly scattered in the entire colloidal sphere, which is different from some results reported.[28,29] After calcination at 600 °C to completely remove organic residues, the morphology of spheres remains unchanged and the size of the spheres obviously shrinks, and their most probable diameter decreases from 110 to 80 nm (Figure S1). Also, the CeO_2 size increases a bit (Figure 1c), and its XRD peaks strengthened to some extent (Figure 1g). In the HRTEM micrograph of calcined Pd−CeO_2 CASs (Figure 1d), the lattice fringes with an interplanar spacing of 0.31 nm is associated with the (111) facet of CeO_2 NPs, and the obvious lattice discontinuities can be observed, which characterizes further the nanosized CeO_2 and the possible lattice strain. Figure 1e is the magnified picture of a single sphere and well demonstrates that ultrasmall Pd clusters (indicated by white arrows) are embedded in the assembled CeO_2 NPs, resulting in a strong interaction between Pd clusters and CeO_2 NPs.

To further confirm the close interaction between Pd and CeO_2 components, XPS was applied to investigate the valence state of Ce and Pd. As shown in Figure 2A, the peaks at BEs of 336.8 and 337.9 eV can be attributed to the dispersed PdO clusters and the Pd−O−Ce structure, respectively, which clearly demonstrated that the Pd species in the Pd−CeO_2 CASs interacted closely with CeO_2 nanocrystals. The Ce 3d XPS spectra in Figure 2B showed a valence variation before and after calcination. The as-prepared sample possesses more Ce^{3+} species that is caused by ethylene glycol during the synthesis, and after thermal treatment, the oxidation of Ce^{3+} to Ce^{4+} obviously occurred, indicating a thermal-induced crystallization process.

The N_2 adsorption/desorption isotherms of the as-synthesized Pd−CeO_2 CASs before and after calcination at 600 °C are shown in Figure 3. In the low relative pressure region, the curves reflect a microporous structure, which may be caused by the stacking of nanocrystals that assembled the spheres. A hysteresis, typical of type IV, appeared in the high relative pressure region, indicating a relatively large pore structure, which is likely caused by the stacking of spheres. The surface area of the sample before and after being calcined at 600 °C is 89 and 80 m^2/g, respectively, which is larger than that of the core−shell Pt/Pd@CeO_2 spheres reported.[28,33]

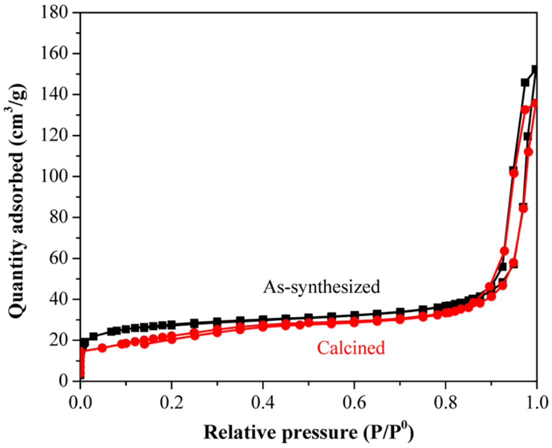

Figure 3. N_2 adsorption/desorption isotherms of the as-synthesized and calcined Pd−CeO_2 CASs at 600 °C.

The formation mechanism of Pd−CeO_2 CASs can be discussed in detail based on the time-controlled experiments. Followed by the visual variation of the reaction system, the formation process undergoes three stages, that is, the nucleation of Pd clusters, formation of CeO_2 nanocrystals, and self-assembly of these two components.

First, the brown transparent solution gradually turned black after 20−30 min of the reaction when the temperature ramped up to 130 °C, indicating the possible formation of Pd clusters in the solution. To verify this assumption, we characterized the solid sample formed for 1.5 h. As shown in Figure 4, the sheetlike structure and ultrasmall Pd clusters coexisted in the sample, but no lattice fringes can be observed. Also, the elemental analysis shows that this sample is consisted of C, H, O, N, Ce, and Pd elements (Table S1). The XRD results (Figure 4f) show that it is a Ce−glycolate-like inorganic−organic network structure and was caused by the Ce ions interacted with acetic acid and ethylene glycol at 130 °C. The FT-IR spectrum (Figure S2) also confirmed that the Ce ions have bonded with ethylene glycol and acetic acid on the basis of the typical IR absorption peaks at 1562 cm^{-1} ν(OCO), 2942, and 2895 cm^{-1} ν(C−H) C_2H_4.[34]

With the increase in the synthesis time, the hydrolysis of Ce species was gradually promoted, and the subsequent self-assembly of nucleated CeO_2 nanocrystals formed the primary spheres (Figure 4b−d). After 10 h of the synthesis reaction, the black transparent solution gradually became blurred, indicating the initial formation of the CeO_2 structure. As shown in Figure 4c,d, the primary CAS and CeO_2 nuclei can coexist simultaneously. Finally, the Pd clusters and CeO_2 nanocystals coassembled into the Pd−CeO_2 hybrid structure (Figure 4e). The XRD patterns in Figure 4f can well reflect the structure change of different intermediate compounds formed in the fabrication process of Pd−CeO_2 CASs.

To obtain a highly dispersible Pd−CeO_2 hybrid structure in a one-pot fashion, the key is to tune the reaction rates for different chemical processes; that is, the balance between the slow hydrolysis of the Ce precursor, Pd-cluster formation, and self-assembled process should be critically controlled, which can be well achieved with the help of surfactants and cosolvents. To clarify the effect of each reagent on the synthetic results, we also designed a series of component-controlled experiments.

(1) We tested the essential role of ammonia hydroxide, acetic acid, and $N(CH_3)_4OH$ in the synthesis of Pd−CeO_2 CASs. When metal salt precursors were added in the solution including acetic acid and $N(CH_3)_4OH$ but without ammonia hydroxide, the obtained synthesis solution was transparent black after 15 h, and only the reduction of Pd^{2+} to Pd^0 occurred and no assembled CeO_2 nanocrystal spheres formed. This was verified by the typical Pd peaks in the XRD pattern of the obtained product (Figure S3).

(2) When the amount of $NH_3·H_2O$ was increased 2-fold up to 0.8 mL, the solution immediately became opaque at 70−80 °C, indicating that a large amount of CeO_2 crystals formed very quickly and its nucleation could not be controlled. The obtained spheres would severely conjugate one another, and the bulklike structure formation was inevitable (TEM image shown in Figure S4). These phenomena confirmed the inevitable role of an appropriate amount of $NH_3·H_2O$, which functions as a pH regulator and affects the hydrolysis rate of Ce ions.

(3) Although $NH_3·H_2O$ is indispensable in the successful fabrication of Pd−CeO_2 CASs, its role can be played only in the presence of acetic acid. Without the addition of this organic acid, the produced Pd particles would aggregate, and CeO_2 nanocrystals could not be well self-assembled into spheres (TEM image shown in Figure S5). It was reported recently that appropriate amounts of formic acid and ammonia hydroxide could be used as a formic acid/ammonium formate buffer solution to effectively control the OH^- concentration.[35] We consider that the acetic

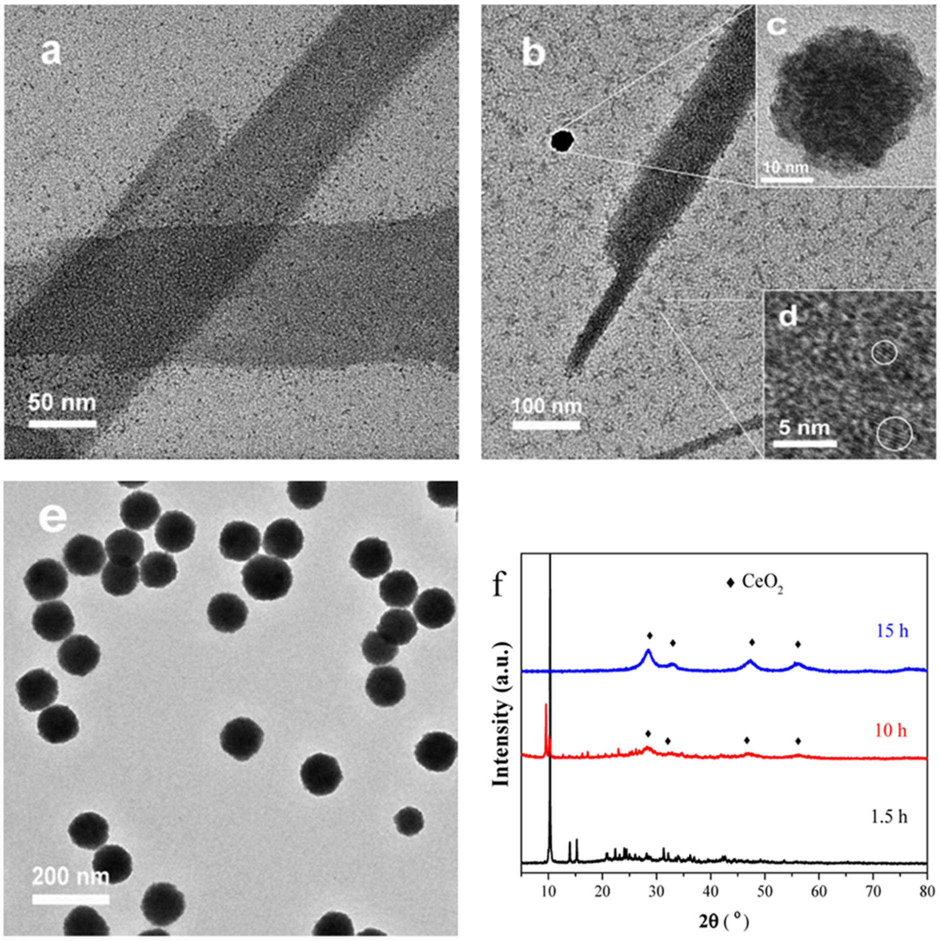

Figure 4. TEM images of the sample formed for (a) 1.5 h, (b−d) 10 h ((c) primary Pd−CeO_2 CAS and (d) CeO_2 nuclei), (e) 15 h, and (f) their XRD patterns.

acid/ammonium acetate plays the similar role in the fabrication of Pd−CeO_2 CASs by tuning the reaction process.

(4) $N(CH_3)_4OH$ was commonly used as a pH regulator as well as a dispersing agent in the synthetic process, which was reported in the synthesis of aqueous dispersible CeO_2 NPs.[36] PVP helps to stabilize Pd clusters against aggregation. If PVP was not added, the black precipitate would be formed and stuck at the flask bottom when the synthesis reaction occurred at 130 °C for a short time.

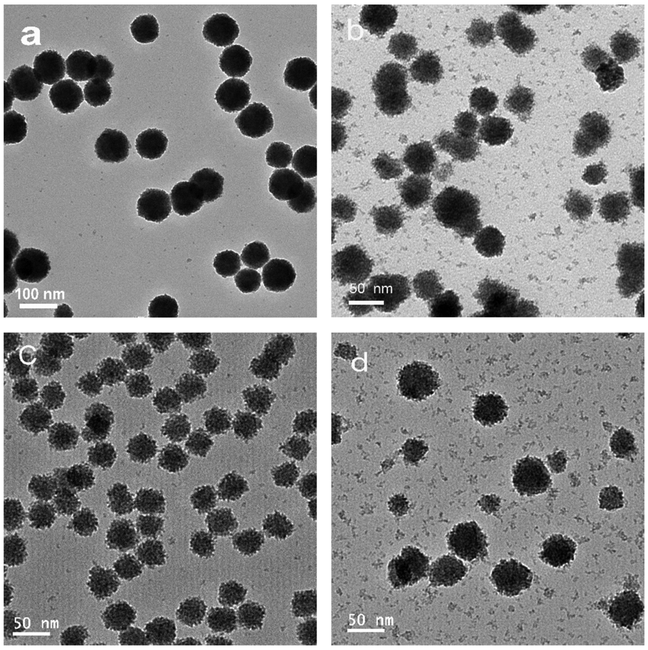

Figure 5. TEM images of the as-prepared (a) Pt−CeO_2 CASs, (b) Cu−CeO_2 CASs, (c) Co−CeO_2 CASs, and (d) Mn−CeO_2 CASs.

On the basis of the above results, each reagent is necessary and its dosage needs to be carefully controlled or balanced to obtain the dispersible Pd−CeO_2 CASs. To our knowledge, it is difficult to design and prepare noble metal- or transition metal-incorporated CeO_2 hybrid nanospheres by a universal method. However, we luckily found that the present approach of structural design could be well used to synthesize other CAS architectures. For example, platinum and some common transition metals (Cu, Mn, and Co) can be easily introduced into CeO_2 CASs by slight changes of experimental conditions. As shown in Figure 5, the diameter of the as-prepared Pt−CeO_2 CASs is nearly the same as that of Pd−CeO_2 CASs, and they are mainly composed of ultrasmall CeO_2 nanocrystallites, and no Pt NPs can be observed. The XPS analysis indicates that the Pt species existed in an ionic state (Figure S6), confirming the highly dispersed Pt species in Pt−CeO_2 CASs. For transition metal-incorporated M−CeO_2 CASs (M = Cu, Co, Mn), their sphere diameters are less than 50 nm, and their XRD profiles showed only the characteristic diffraction peaks of the fluorite

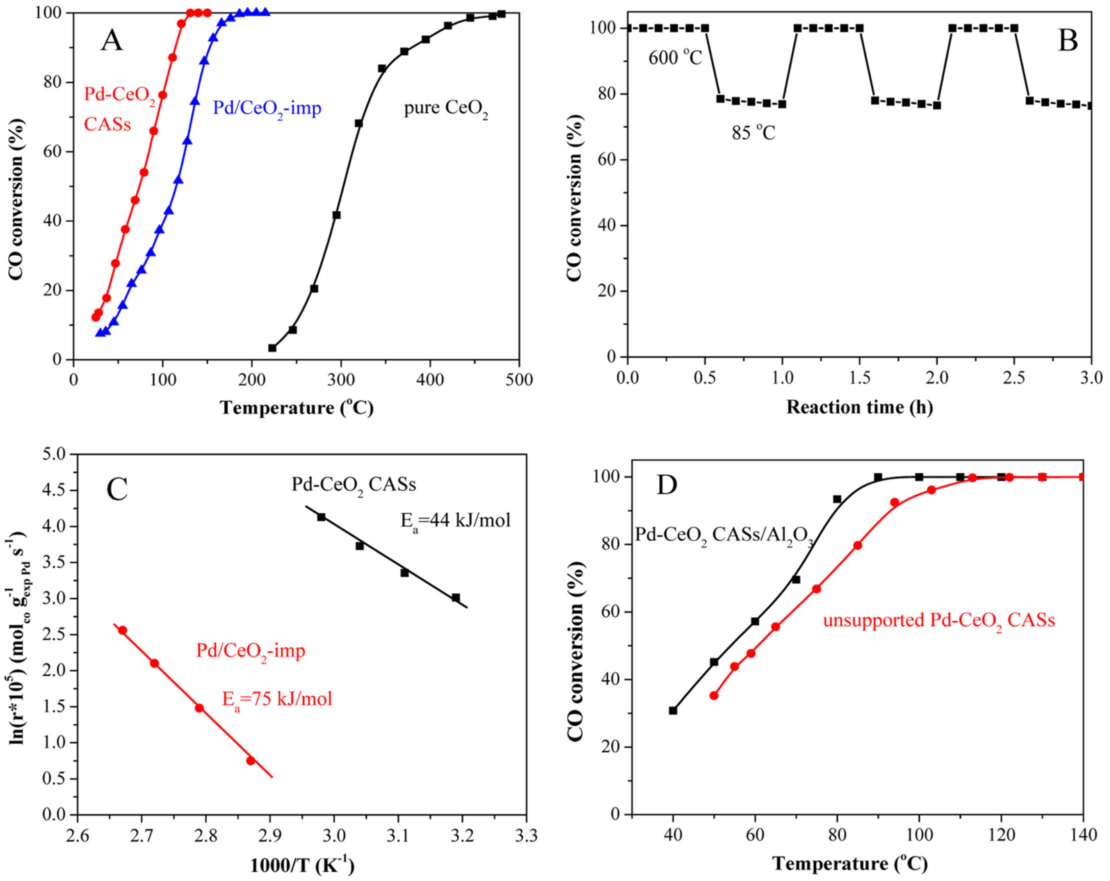

Figure 6. (A) Catalytic activities of Pd−CeO$_2$ CASs, Pd/CeO$_2$-imp, and pure CeO$_2$ CASs for CO oxidation and (B) the cycling testing of Pd−CeO$_2$ CASs at alternating temperatures of 600 and 85 °C (the feed gas of 1 vol % CO in air and GHSV of 40 000 mL/(g_{cat}·h)). (C) Kinetic data of CO oxidation on Pd−CeO$_2$ CASs and Pd/CeO$_2$-imp (CO conversion was kept <10%). (D) CO oxidation activities of unsupported Pd−CeO$_2$ CASs and subsequently supported Pd−CeO$_2$ CAS/Al$_2$O$_3$ catalysts (GHSV of 60 000 mL/(g_{cat}·h)).

CeO$_2$ structure (Figure S7), which indicates that the successful incorporation into the CASs. Their transition metal contents were measured by the EDS analysis (Figure S8), and Cu/Ce (at %) = 9.5, Co/Ce = 4.2, and Mn/Ce = 6.5.

To investigate the catalytic performance of the Pd−CeO$_2$ CAS material, the CO catalytic oxidation was used as the model reaction. For comparison, we tested the catalytic activities of the Pd/CeO$_2$-imp sample prepared by the impregnation method and pure CeO$_2$ for CO oxidation. As shown in Figure 6A, Pd−CeO$_2$ CASs exhibited the best catalytic activity, and the temperature (T_{100}) of 100% CO conversion is around 125 °C, which is much lower than that of the Pd/CeO$_2$-imp catalyst (190 °C). T_{10}, T_{50}, and T_{90} (the reaction temperatures of 10, 50, and 90% CO conversions) were shown in Table 1. Besides, the Pd−CeO$_2$ CASs also showed a good thermal stability after the cycling testing 3 times at 600 and 85 °C (Figure 6B). A decline of 2−3% CO conversion can be observed, which can be explained by the minor accumulation of carbonate species on the catalyst surface.[37,38] The TEM image (Figure S9) showed that the morphology of Pd−CeO$_2$ CASs was well maintained and no agglomeration occurred after the cycling testing 3 times. A recent study on similar the Pd@CeO$_2$ nanostructure showed that at medium-high temperature and an oxidizing atmosphere cerium could be quite volatile and some new structural features would appear, including highly dispersed SiO$_2$−CeO$_x$ species and rather bigger CeO$_2$ particles.[39] Therefore, after the relatively long time utilization of Pd−CeO$_2$ CASs in the cycling experiment at 600 °C, we cannot neglect their possible structural change, although the morphology of Pd−CeO$_2$ CASs could be well maintained. Also, further detailed characterization and analysis are needed.

Table 1. Pd Contents, Pd Dispersions (D_{Pd}), and the Catalytic Activities of Pd−CeO$_2$ CASs and Pd/CeO$_2$-Imp for CO Oxidation

sample	Pd content (wt %)[a]	D_{Pd} (%)[b]	T_{10} (°C)	T_{50} (°C)	T_{90} (°C)	TOF (s^{-1})[c]
Pd−CeO$_2$ CASs	1.1	28	24	74	113	0.051
Pd/CeO$_2$-imp	0.97	34	48	115	150	0.026

[a] Pd content was measured by ICP. [b] Pd dispersion was determined by CO chemisorption. [c] TOFs were measured at 60 °C.

The kinetic data of CO oxidation on Pd−CeO$_2$ CASs and Pd/CeO$_2$-imp are shown in Figure 6C. The results showed that the Pd−CeO$_2$ CASs exhibited much higher catalytic activity (or much higher reaction rate) than the Pd/CeO$_2$-imp catalyst. Also, the apparent activation energy (E_a) of the Pd−CeO$_2$ CAS catalyst was 44 kJ/mol, which is much lower than that (E_a = 75 kJ/mol) of the Pd/CeO$_2$-imp catalyst. We have further calculated the TOF at 60 °C; the TOF of the Pd/CeO$_2$-imp catalyst is ~0.026 s^{-1}, and the TOF of Pd−CeO$_2$ CASs is ~0.051 s^{-1} (Table 1), which also confirmed that the Pd−CeO$_2$ CAS nanocatalyst possessed higher catalytic activity than the Pd/CeO$_2$-imp catalyst for CO oxidation under the same reaction condition. Furthermore, we listed TOFs of reported Pd−CeO$_2$

catalysts at certain temperatures for CO oxidation in Table 2, and the results show that the catalytic activity of Pd−CeO_2 CASs is higher than that reported.

Table 2. Catalytic Activities of Pd−CeO_2 Catalysts for CO Oxidation

catalyst	reaction temperature (°C)	TOF (s^{-1})	ref
Pd/CeO_2-nanorod	50	0.04	38
Pd/CeO_2	97	0.017	41
Pd−mesoporous CeO_2	20	0.024	42
PdO−CeO_2/SiO_2	150	0.038	43
PdO/$Ce_{1-x}Pd_xO_{2-\delta}$	140	0.036	44
Pd/CeO_2 model catalyst	80	∼0.04	45
Pd−CeO_2 CASs	60	0.051	this work

To investigate and compare the differences of reducibility and an interaction of Pd species with CeO_2 between the Pd−CeO_2 CASs and Pd/CeO_2-imp catalyst, H_2-TPR was used to test these two catalysts, and the results are shown in Figure 7. In the two TPR profiles, there are two peaks at below 200 °C, but their intensities and positions are different. We may attribute the first peak at below 200 °C to the reduction of PdO species and the second to the reduction of the Pd^{2+}−O−Ce^{4+} linkage structure.[37,40] The calculated H_2 consumption of the first peak in Pd/CeO_2-imp at 60 °C is ∼104 μmol/g and is close to the theoretical value (88 μmol/g) for PdO reduction to metallic Pd. For Pd−CeO_2 CASs, the H_2 consumption of the first peak is much lower than its theoretical value. This is because of the fact that in the Pd/CeO_2-imp sample the Pd species existed mostly in a form of PdO by the impregnation process with few Pd^{2+} incorporated into the CeO_2 support; in the Pd−CeO_2 CAS sample, most Pd species formed a solid solution with CeO_2 nanocrystallites produced during the solvothermal process. Moreover, we can observe a very small negative peak in the TPR curves of two samples (∼60 °C for Pd−CeO_2 CASs and ∼80 °C for Pd/CeO_2-imp), which could be attributed to the decomposition of PdH_x species.

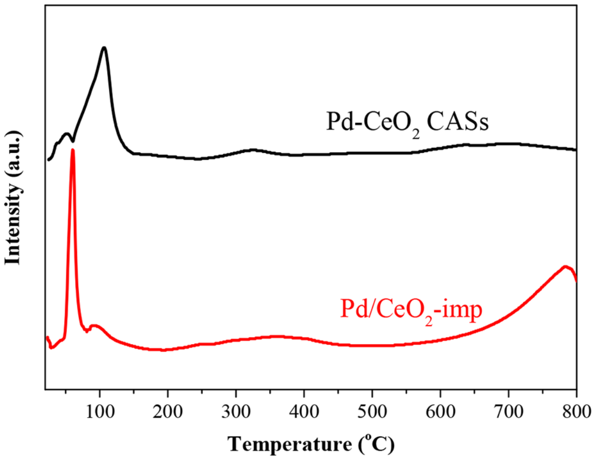

Figure 7. H_2-TPR profiles of 1.1 wt % Pd−CeO_2 CASs and 1 wt % Pd/CeO_2-imp.

In the reduction peaks at <200 °C, the total H_2 consumption of Pd/CeO_2-imp and Pd−CeO_2 CASs is ∼211 and 427 μmol/g, respectively, which are higher than that when reducing PdO to Pd. Thus, it is inevitable that the reduction peak may contain simultaneous reduction of Ce^{4+} ions near Pd species. This is because that the presence of noble metals can promote the reduction of metal oxides by the H_2 spillover from the metal to the oxide support, as well as the increase of oxygen vacancies on the ceria support. With more Pd^{2+} ions incorporated into the CeO_2 nanocrystals in the synthesis process, the Pd−CeO_2 CASs possessed more oxygen vacancy defects; thus, more Ce^{4+} can be easily reduced at lower temperatures.

For the reduction peak at 320−370 °C, it should be attributed to the reduction of surface lattice oxygen. In the Pd−CeO_2 CAS catalyst, because the Pd^{2+}−O−Ce^{4+} linkage structure (Pd^{2+} incorporated into CeO_2) existed besides highly dispersed PdO clusters, part of surface lattice oxygen was reduced at <200 °C, which was promoted by the reduction of Pd^{2+} ions, resulting in the decrease in the peak area at 324 °C. The reduction peak at >700 °C is ascribed to the reduction of bulk CeO_2 and affected by the CeO_2 particle size. The average particle size of CeO_2 is 5−6 nm for Pd−CeO_2 CASs, and for the Pd/CeO_2-imp catalyst, the particle size of its commercial nanosized CeO_2 powder is over 20 nm. This leads to a distinguishing difference in their H_2-TPR profiles. With the decrease of the CeO_2 particle size, more surface oxygen existed in the Pd−CeO_2 CASs, so the reduction of bulk CeO_2 decreased obviously.[46]

As shown in the characterization results above for the Pd−CeO_2 CAS catalyst, the active Pd species existed mainly in highly dispersed PdO clusters and Pd^{2+} incorporated into CeO_2 (Pd^{2+}−O−Ce^{4+} linkage structure), which act the active sites for CO oxidation. In this Pd−CeO_2 CAS hybrid spheres, the enhanced catalytic activity can be attributed to the synergetic effect provided by two aspects: the surface dispersed PdO clusters are more active for CO adsorption, and the Pd^{2+} ions incorporated into the CeO_2 lattice creates more oxygen vacancies, which are beneficial to oxygen activation in CO oxidation. For the Pd/CeO_2-imp catalyst, the O_2 activation might be weaker than that for the Pd−CeO_2 CAS catalyst because of the lack of oxygen vacancies on the surface, resulting in its lower catalytic activity for CO oxidation.

One of the advantages of ordered hybrid nanocatalysts is that every independent unit can be viewed as an individual active reactor in the catalytic reaction, and it is helpful to load these nanocatalysts on high-surface area supports to further improve the overall catalytic performance.[26,29] Hence, we prepared the Pd−CeO_2 CAS/Al_2O_3 by a simple process (seen in the Experimental Section). The results showed that Pd−CeO_2 CAS particles could be uniformly supported on the Al_2O_3 carrier (TEM image, Figure S10). The BET surface area (144 m^2/g) of Pd−CeO_2 CAS/Al_2O_3 is higher than that (80 m^2/g) of the unsupported one, and their N_2 adsorption/desorption isotherms are shown in Figure S11. After Pd−CeO_2 CASs were supported, their dispersion was improved, resulting in an increase in their catalytic performance (Figure 6D). Besides, this procedure was also applied to fabricate the Pt−CeO_2 CAS/Al_2O_3 sample; as shown in Figure S12, CO was completely converted to CO_2 over this Pt catalyst at 115 °C, which has a higher catalytic activity than those reported for the Pt catalysts for CO oxidation.[33,47,48]

4. CONCLUSIONS

In summary, we have developed a facile one-pot method to successfully synthesize Pd−CeO_2 CASs, in which ultrasmall Pd clusters are embedded in the CeO_2 colloidal assembly. The synthesis process involves careful control of Pd-cluster formation, the Ce^{3+} hydrolysis rate, and the subsequent assembly process. Each surfactant/cosolvent is necessary for the successful fabrication of this material. For CO oxidation, this Pd−CeO_2 CAS sample shows a much higher catalytic activity compared with the Pd/CeO_2 catalyst prepared by the impregnation method. The enhanced catalytic activity can be attributed to the maximized Pd−CeO_2 interface of this ordered hybrid spheres. Moreover, after the Pd−CeO_2 CAS sample was simply supported on alumina, its overall catalytic performance can be further improved, for instance, the temperature of the CO complete conversion was only around 90 °C. Because this Pd−CeO_2 CAS also exhibit a relatively high thermal stability, it can potentially be valuable for other hydrocarbon abatement processes, such as methane or propane combustion. The successful synthesis of M−CeO_2 CASs (M = Pt, Cu, Mn, Co) shows further that this method is a new and ideal approach for fabricating active and stable ceria-based materials.

■ ASSOCIATED CONTENT

Supporting Information

The Supporting Information is available free of charge on the ACS Publications website at DOI: 10.1021/acsomega.6b00050.

> Size distributions of Pd−CeO_2 CASs, FT-IR spectrum and composition of the sample prepared for 1.5 h, XRD profile and TEM images of the sample prepared at 130 °C for 15 h with different additives, XPS spectrum of Pt−CeO_2 CASs, XRD profiles and EDS spectra of M−CeO_2 CASs, TEM images of cycled Pd−CeO_2 CASs and supported Pd−CeO_2 CAS/Al_2O_3, N_2 adsorption/desorption isotherms of Al_2O_3 and Pd−CeO_2 CAS/Al_2O_3, and activity profiles of Pt−CeO_2 CASs and Pt−CeO_2 CAS/Al_2O_3 (PDF)

■ AUTHOR INFORMATION

Corresponding Author

*E-mail: gzhlu@ecust.edu.cn. Fax: +86-21-64252923.

Notes

The authors declare no competing financial interest.

■ ACKNOWLEDGMENTS

This project was financially supported by the National Basic Research Program of China (2013CB933201), the National Natural Science Foundation of China (21273150), the National High Technology Research and Development Program of China (2011AA03A406, 2012AA062703), the Commission of Science and Technology of Shanghai Municipality (15DZ1205305), and the Fundamental Research Funds for the Central Universities (WJ1514020).

■ REFERENCES

(1) Buchwald, S. L. Cross Coupling. *Acc. Chem. Res.* **2008**, *41*, 1439.

(2) Garciá-Melchor, M.; Braga, A. A. C.; Lledós, A.; Ujaque, G.; Maseras, F. Computational Perspective on Pd-catalyzed C−C Cross-Coupling Reaction Mechanisims. *Acc. Chem. Res.* **2013**, *46*, 2626−2634.

(3) Peng, H.-C.; Xie, S.; Park, J.; Xia, X.; Xia, Y. Quantitative Analysis of the Coverage Density of Br^- Ions on Pd{100} Facets and Its Role in Controlling the Shape of Pd Nanocrystals. *J. Am. Chem. Soc.* **2013**, *135*, 3780−3783.

(4) Choi, S.; Shao, M.; Lu, N.; Ruditskiy, A.; Peng, H.-C.; Park, J.; Guerrero, S.; Wang, J.; Kim, M. J.; Xia, Y. Synthesis and Characterization of Pd@Pt−Ni Core−Shell Octahedra with High Activity Towards Oxygen Reduction. *ACS Nano* **2014**, *8*, 10363−10371.

(5) Miyaura, N.; Suzuki, A. Palladium-Catalyzed Cross-Coupling Reactions of Organoboron Compounds. *Chem. Rev.* **1995**, *95*, 2457−2483.

(6) Xue, L.; Lin, Z. Theoretical Aspects of Palladium-Catalysed Carbon−Carbon Cross-Coupling Reactions. *Chem. Soc. Rev.* **2010**, *39*, 1692−1705.

(7) Cargnello, M.; Jaén, J. J. D.; Garrido, J. C. H.; Bakhmutsky, K.; Montini, T.; Gaméz, J. J. C.; Gorte, R. J.; Fornasiero, P. Exceptional Activity for Methane Combustion over Modular Pd@CeO_2 Subunits on Functionalized Al_2O_3. *Science* **2012**, *337*, 713−717.

(8) Wang, J.; Chen, H.; Hu, Z.; Yao, M.; Li, Y. A Review on the Pd-Based Three-Way Catalysts. *Catal. Rev.* **2015**, *57*, 79−144.

(9) Chen, X.; Wu, G.; Chen, J.; Chen, X.; Xie, Z.; Wang, X. Synthesis of "Clean" and Well-Dispersive Pd Nanoparticles with Excellent Electrocatalytic Property on Graphene Oxide. *J. Am. Chem. Soc.* **2011**, *133*, 3693−3695.

(10) Cheong, S.; Watt, J. D.; Tilley, R. D. Shape Control of Platinum and Palladium Nanoparticles for Catalysis. *Nanoscale* **2010**, *2*, 2045−2053.

(11) Martins, J.; Batail, N.; Silva, S.; Rafik-Clement, S.; Karelovic, A.; Debecker, D. P.; Chaumonnot, A.; Uzio, D. CO_2 Hydrogenation with Shape-Controlled Pd Nanoparticles Embedded in Mesoporous Silica: Elucidating Stability and Selectivity Issues. *Catal. Commun.* **2015**, *58*, 11−15.

(12) Wang, Y.; Choi, S.; Zhao, X.; Xie, S.; Peng, H.-C.; Chi, M.; Huang, C. Z.; Xia, Y. Polyol Synthesis of Ultrathin Pd Nanowires via Attachment-Based Growth and Their Enhanced Activity towards Formic Acid Oxidation. *Adv. Funct. Mater.* **2014**, *24*, 131.

(13) Montini, T.; Melchionna, M.; Monai, M.; Fornasiero, P. Fundamental and Catalytic Applications of CeO_2-Based Materials. *Chem. Rev.* **2016**, *116*, 5987−6041.

(14) Zhang, Z. X.; Jiang, Z.; Shangguan, W. Low-temperature Catalysts for VOCs Removal in Technology and Application: A State-of-the-Art Review. *Catal. Today* **2016**, *264*, 270−278.

(15) Vilé, G.; Bridier, B.; Wichert, J.; Pérez-Ramírez, J. Ceria in Hydrogenation Catalysis: High Selectivity in the Conversion of Alkynes to Olefins. *Angew. Chem., Int. Ed.* **2012**, *51*, 8620−8623.

(16) Zhang, S.; Chang, C.-R.; Huang, Z.-Q.; Li, J.; Wu, Z.; Ma, Y.; Zhang, Z.; Wang, Y.; Qu, Y. High Catalytic Activity and Chemoselectivity of Sub-Nanometric Pd Clusters on Porous Nanorods of CeO_2 for Hydrogenation of Nitroanenes. *J. Am. Chem. Soc.* **2016**, *138*, 2629−2637.

(17) Zhang, S.; Chang, C. R.; Huang, Z. Q.; Ma, Y. Y.; Gao, W.; Li, J.; Qu, Y. Q. Visible-Light-Activated Suzuki-Miyaura Coupling Reactions of Aryl Chlorides over the Multifunctional Pd/Au/Porous Nanorods of CeO_2 Catalysis. *ACS Catal.* **2015**, *5*, 6481−6488.

(18) Tan, H.; Wang, J.; Yu, S.; Zhou, K. Support-Morphology-Dependent Catalytic Activity of Pd/CeO_2 for Formaldehyde Oxidation. *Environ. Sci. Technol.* **2015**, *49*, 8675−8682.

(19) Li, G.; Wang, Q.; Zhao, B.; Zhou, R. Promoting Effect of Synthesis Method on the Property of Nickel Oxide Doped CeO_2−ZrO_2 and the Catalytic Behaviour of Pd-only Three-way Catalysts. *Appl. Catal., B* **2011**, *105*, 151−162.

(20) Zhang, N.; Xu, Y.-J. Aggregation- and Leaching-Resistant, Reusable, and Multifunctional Pd@CeO_2 as a Robust Nanocatalyst Achieved by a Hollow Core−Shell Strategy. *Chem. Mater.* **2013**, *25*, 1979−1988.

(21) Chen, C.; Fang, X.; Wu, B.; Huang, L.; Zheng, N. A Multi-Yolk−Shell Structured Nanocatalyst Containing Sub-10 nm Pd Nanoparticles in Porous CeO_2. *ChemCatChem* **2012**, *4*, 1578−1586.

(22) Zhang, N.; Liu, S.; Fu, X.; Xu, Y.-J. A Simple Strategy for Fabrication of "Plum-Pudding" Type Pd@CeO_2 Semiconductor Nanocomposite as a Visible-Light-Driven Photocatalyst for Selective Oxidation. *J. Phys. Chem. C* **2011**, *115*, 22901−22909.

(23) Cargnello, M.; Montini, T.; Polizzi, S.; Wieder, N. L.; Gorte, R. J.; Graziani, M.; Fornasiero, P. Novel Embedded Pd@CeO_2 Catalysts: A Way to Active and Stable Catalysts. *Dalton Trans.* **2010**, *39*, 2122−2127.

(24) Song, S.; Wang, X.; Zhang, H. CeO_2-Encapsulated Noble Metal Nanocatalysts: Enhanced Activity and Stability for Catalytic Application. *NPG Asia Mater.* **2015**, *7*, No. e179, DOI: 10.1038/am.2015.27.

(25) Cargnello, M.; Wieder, N. L.; Montini, T.; Gorte, R. J.; Fornasiero, P. Synthesis of Dispersible Pd@CeO_2 Core−Shell Nanostructures by Self-Assembly. *J. Am. Chem. Soc.* **2010**, *132*, 1402−1409.

(26) Adijanto, L.; Bennett, D. A.; Chen, C.; Yu, A. S.; Cargnello, M.; Fornasiero, P.; Gorte, R. J.; Vohs, J. M. Exceptional Thermal Stability of Pd@CeO_2 Core−Shell Catalyst Nanostructures Grafted onto an Oxide Surface. *Nano Lett.* **2013**, *13*, 2252−2257.

(27) Monai, M.; Montini, T.; Chen, C.; Fonda, E.; Gorte, R. J.; Fornasiero, P. Methane Catalytic Combustion over Hierarchical Pd@CeO_2/Si-Al_2O_3: Effect of the Presence of Water. *ChemCatChem* **2015**, *7*, 2038−2046.

(28) Wang, X.; Liu, D.; Li, J.; Zhen, J.; Wang, F.; Zhang, H. γ-Al_2O_3 Supported Pd@CeO_2 Core@Shell Nanospheres: Salting-out Assisted Growth and Self-assembly, and Their Catalytic Performance in CO Oxidation. *Chem. Sci.* **2015**, *6*, 2877−2884.

(29) Wang, X.; Zhang, Y.; Song, S.; Yang, X.; Wang, Z.; Jin, R.; Zhang, H. L-Arginine-Triggered Self-Assembly of CeO_2 Nanosheets on Palladium Nanoparticles in Water. *Angew. Chem., Int. Ed.* **2016**, *55*, 4542−4546.

(30) Du, C.; Guo, Y.; Guo, Y.; Gong, X.-Q.; Lu, G. Polymer-templated synthesis of hollow Pd−CeO_2 nanocomposite spheres and their catalytic activity and thermal stability. *J. Mater. Chem. A* **2015**, *3*, 23230−23239.

(31) Chen, C.; Nan, C.; Wang, D.; Su, Q.; Duan, H.; Liu, X.; Zhang, L.; Chu, D.; Song, W.; Peng, Q.; Li, Y. Mesoporous Multicomponent Nanocomposite Colloidal Spheres: Ideal High-Temperature Stable Model Catalysts. *Angew. Chem., Int. Ed.* **2011**, *50*, 3725−3729.

(32) Wang, F.; Li, W.; Feng, X.; Liu, D.; Zhang, Y. Decoration of Pt on Cu/Co double-doped CeO_2 nanospheres and their greatly enhanced catalytic activity. *Chem. Sci.* **2016**, *7*, 1867−1873.

(33) Wang, X.; Liu, D.; Song, S.; Zhang, H. Pt@CeO_2 Multicore@Shell Self-Assembled Nanospheres: Clean Synthesis, Structure Optimization, and Catalytic Applications. *J. Am. Chem. Soc.* **2013**, *135*, 15864−15872.

(34) Aguirre-Díaz, L. M.; Gándara, F.; Iglesias, M.; Snejko, N.; Gutiérrez-Puebla, E.; Monge, M. A. Tunable Catalytic Activity of Solid Solution Metal−Organic Frameworks in One-Pot Multicomponent Reactions. *J. Am. Chem. Soc.* **2015**, *137*, 6132−6135.

(35) Zhang, W.; Chi, Z.-X.; Mao, W.-X.; Lv, R.-W.; Cao, A.-M.; Wan, L.-J. One-Nanometer-Precision Control of Al_2O_3 Nanoshells through a Solution-Based Synthesis Route. *Angew. Chem., Int. Ed.* **2014**, *53*, 12776−12780.

(36) Sato, K.; Arai, M.; Valmalette, J.-C.; Abe, H. Surface Capping-Assisted Hydrothermal Growth of Gadolinium-Doped CeO_2 Nanocrystals Dispersible in Aqueous Solutions. *Langmuir* **2014**, *30*, 12049−12056.

(37) Zhou, Y.; Lawrence, N. J.; Wu, T.-S.; Liu, J.; Kent, P.; Soo, Y.-L.; Cheung, C. L. Pd/CeO_{2-x} Nanorod Catalyst for CO Oxidation: Insights into the Origin of Their Regenerative Ability at Room Temperature. *ChemCatChem* **2014**, *6*, 2937−2946.

(38) Hu, Z.; Liu, X.; Meng, D.; Guo, Y.; Guo, Y.; Lu, G. Effect of Ceria Crystal Plane on the Physicochemical and Catalytic Properties of Pd/Ceria for CO and Propane Oxidation. *ACS Catal.* **2016**, *6*, 2265−2279.

(39) Zhang, S.; Chen, C.; Cargnello, M.; Fornasiero, P.; Gorte, R. J.; Graham, G. W.; Pan, X. Dynamic Structural Evolution of Supported Palladium−Ceria Core−Shell Catalysts Revealed by In Situ Electron Microscopy. *Nat. Commun.* **2015**, *6*, 7778.

(40) Kurnatowska, M.; Kepinski, L.; Mista, W. Structure Evolution of Nanocrystalline $Ce_{1-x}Pd_xO_{2-y}$ Mixed Oxide in Oxidizing and Reducing Atmosphere: Reduction-Induced Activity in Low-temperature CO Oxidation. *Appl. Catal., B* **2012**, *117−118*, 135−147.

(41) Satsuma, A.; Osaki, K.; Yanagihara, M.; Ohyama, J.; Shimizu, K. Activity controlling factors for low-temperature oxidation of CO over supported Pd catalysts. *Appl. Catal., B* **2013**, *132−133*, 511−518.

(42) Li, G.; Li, L.; Yuan, Y.; Shi, J.; Yuan, Y.; Li, Y.; Zhao, W.; Shi, J. Highly Efficient Mesoporous Pd/CeO_2 Catalyst for Low Temperature CO Oxidation Especially Under Moisture Condition. *Appl. Catal. B* **2014**, *158−159*, 341−347.

(43) Wang, S.-Y.; Li, N.; Zhou, R.-M.; Jin, L.-Y.; Hu, G.-S.; Lu, J.-Q.; Luo, M.-F. Comparing the CO Oxidation Activity of free PdO and Pd^{2+} Ions over PdO-CeO_2/SiO_2 Catalysts. *J. Mol. Catal. A: Chem.* **2013**, *374−375*, 53−58.

(44) Meng, L.; Jia, A.-P.; Lu, J.-Q.; Luo, L.-F.; Huang, W.-X.; Luo, M.-F. Synergetic Effects of PdO Species on CO Oxidation over PdO−CeO_2 Catalysts. *J. Phys. Chem. C* **2011**, *115*, 19789−19796.

(45) Cargnello, M.; Doan-Nguyen, V. V. T.; Gordon, T. R.; Diaz, R. E.; Stach, E. A.; Gorte, R. J.; Fornasiero, P.; Murray, C. B. Control of Metal Nanocrsytal Size Reveals Metal-Support Interface Role for Ceria Catalysts. *Science* **2013**, *341*, 771−773.

(46) Xu, J.; Harmer, J.; Li, G.; Chapman, T.; Collier, P.; Longworth, S.; Tsang, S. C. Size Dependent Oxygen Buffering Capacity of Ceria Nanocrystals. *Chem. Commun.* **2010**, *46*, 1887−1889.

(47) Shang, L.; Bian, T.; Zhang, B.; Zhang, D.; Wu, L.-Z.; Tung, C.-H.; Yin, Y.; Zhang, T. Graphene-Supported Ultrafine Metal Nanoparticles Encapsulated by Mesoporous Silica: Robust Catalysts for Oxidation and Reduction Reactions. *Angew. Chem., Int. Ed.* **2014**, *53*, 250−254.

(48) Zhou, H.-P.; Wu, H.-S.; Shen, J.; Yin, A.-X.; Sun, L.-D.; Yan, C.-H. Thermally Stable Pt/CeO_2 Hetero-Nanocomposites with High Catalytic Activity. *J. Am. Chem. Soc.* **2010**, *132*, 4998−4999.